Published in final edited form as:
Magn Reson Med. 2011 June ; 65(6): 1776–1785. doi:10.1002/mrm.22765.

Magnetic poly(lactide-co-glycolide) (PLGA) and cellulose particles for MRI-based cell tracking

Michael K. Nkansah[a,b], **Durga Thakral**[b], and **Erik M. Shapiro**[a,b,c,d,*]

[a] Department of Biomedical Engineering, Yale University, New Haven, CT 06511, USA

[b] Molecular and Cellular MRI Laboratory, Magnetic Resonance Research Center, 300 Cedar Street, Yale University School of Medicine, New Haven, CT 06510, USA

[c] Department of Diagnostic Radiology, Yale University School of Medicine, New Haven, CT 06520, USA

[d] Yale Stem Cell Center, Yale University School of Medicine, New Haven, CT 06520, USA

Abstract

Biodegradable, superparamagnetic micro- and nanoparticles of poly(lactide-*co*-glycolide) (PLGA) and cellulose were designed, fabricated and characterized for magnetic cell labeling. Monodisperse nanocrystals of magnetite were incorporated into micro- and nanoparticles of PLGA and cellulose with high efficiency using an oil-in-water single emulsion technique. Superparamagnetic cores had high magnetization (72.1 emu/g). The resulting polymeric particles had smooth surface morphology and high magnetite content (43.3 wt% for PLGA and 69.6 wt% for cellulose). While PLGA and cellulose nanoparticles displayed highest r_2* values per millimole of iron (399 $s^{-1}mM^{-1}$ for cellulose and 505 $s^{-1}mM^{-1}$ for PLGA), micron-sized PLGA particles had a much higher r_2* per particle than either. After incubation for a month in citrate buffer (pH 5.5), magnetic PLGA particles lost close to 50% of their initial r_2* molar relaxivity, while magnetic cellulose particles remained intact, preserving over 85% of their initial r_2* molar relaxivity. Lastly, mesenchymal stem cells and human breast adenocarcinoma cells were magnetically labeled using these particles with no detectable cytotoxicity. These particles are ideally suited for non-invasive cell tracking *in vivo* via MRI and due to their vastly different degradation properties, offer unique potential for dedicated use for either short (PLGA-based particles) or long term (cellulose-based particles) experiments.

1. Introduction

Magnetic cell labeling for the purpose of MRI-based cell tracking has been achieved with a variety of iron oxide-based contrast agents [1-3]. Most common among these are ferumoxides or dextran-coated small particles of iron oxide (SPIOs), used clinically to help identify tumors in the liver. Ferumoxides, following intravenous administration, are phagocytosed and metabolized by the Kupffer cells of the liver, which form part of the reticuloendothelial system. Ferumoxides have generated keen interest for magnetic cell labeling mostly because of a clinically approved formulation, Feridex®. Despite this perceived benefit, a serious drawback to their use is the low iron content per particle (less than 0.1% by volume). Thus, cells need to endocytose millions of Ferumoxides particles in order to produce significant contrast [4]. Furthermore the label can be diluted beyond detectable levels as cells proliferate [5].

* Corresponding author. E.M. Shapiro: Magnetic Resonance Research Center, Yale School of Medicine, 300 Cedar Street, TAC N129, New Haven, CT 06519, USA; Tel: +1 (203)785-2899; Fax: +1 (203) 785-6643; erik.shapiro@yale.edu.

As an alternative, commercially available micron-sized iron oxide particles (MPIOs, Bangs Labs) have been used for magnetic cell labeling [4]. MPIOs have several benefits over SPIO for magnetic cell labeling. Firstly, MPIOs contain a much higher percentage of magnetite than Ferumoxides, upwards to 45% by weight [6]. This efficiency in packaging iron allows for higher iron loading with MPIOs [4]. The second benefit is that MPIOs have higher r_2* molar relaxivity than Ferumoxides [7]. This is due to the overall size of the superparamagnetic entity, shifting the relaxation regime further into static dephasing regime [8]. Thirdly, since only a single MPIO is needed to create significant contrast, the magnetic label is not lost during cell division [9]. Lastly, MPIOs are commercially available with fluorescence incorporated into the particle. The perceived downside with MPIOs, however, is that the beads are composed of poly(divinylbenzene), an inert, non-degradable polymer that has not been FDA-approved for use in humans. This may limit any potential clinical utility of inert MPIOs [10]. An ideal particle for MRI-based cell tracking would therefore combine the biocompatibility of dextran-coated nanoparticles with the high iron content of MPIOs and flexibility for fluorescence incorporation.

Biodegradable, polymer encapsulated magnetic particles, using polymers such as poly(lactide-*co*-glycolide) (PLGA) and poly(lactic acid) (PLA), have been fabricated largely for targeted delivery of encapsulated drug payloads and imaging confirmation. However, few studies have concentrated on the fabrication of durable magnetic cell labeling probes, designed to have prolonged intracellular residence. Lee, et al, recently reported on microgel iron oxide nanoparticles with a wide range of hydrodynamic diameters (86-766 nm) and significant magnetite content (up to 82 wt%) for labeling endothelial progenitor cells [11]. In another recent report, Wang, et al, fabricated 100 nm biodegradable poly(DL-lactic acid-*co*-α,β-malic acid)/magnetite nanoparticles for magnetic cell labeling [12]. Particles contained ~18% magnetite with excellent r_2 molar relaxivity (~165 $mm^{-1}sec^{-1}$) and could label human mesenchymal cells in vitro without impairing the ability of stem cells to differentiate. A third example is a report by Lim, et al, where magnetite cores were encapsulated within PLGA at ~ 150 nm total diameter [13]. Excellent MRI properties were measured (r_2 = 161 $mm^{-1}sec^{-1}$) and robust cell labeling was achieved. However, in all three cases, no analysis of the degradation properties of the particles and dissolution of the encapsulated iron was performed. These measurements are crucial in designing particles for clinical translation, both from a safety perspective as well as biophysical and MRI viewpoints. Furthermore, full characterization of particle lifetimes, for different polymers, can help to design particles dedicated for particular uses. For example, in the case of immune cell tracking, where cells do not live very long, a few days at most, the use of particles with rapid degradation would help avoid the detection of false positive MRI contrast when the cell of interest is long gone. Conversely, the use of long lasting particles would be beneficial for stem cell transplants, where the cell of interest is anticipated to live much longer.

Here we describe the fabrication of magnetic and fluorescent, biodegradable micro- and nanoparticles, composed either of PLGA or cellulose. Both polymers are FDA-approved for a variety of uses in humans and commonly employed for drug delivery and oral tablet formulations. Furthermore, these two polymers degrade at substantially different rates, offering the potential to design particle-based MRI cell tracking agents for either short term (PLGA) or long term (cellulose) experiments. As these agents are designed for MRI-based cell tracking, and thus intracellular retention, we characterized longitudinal particle degradation and iron dissolution, both in terms of biophysical processes as well as MRI parameters. Lastly, we demonstrate their capability in labeling cells for MRI-based cell tracking.

2. Materials and Methods

2.1 Synthesis and characterization of magnetite nanocrystals

Magnetite nanocrystals were synthesized via a thermal decomposition of iron oleate [14,15]. 10-nm magnetite nanocrystals were synthesized by heating a mixture of iron oleate (3.6 g; 4 mmol) and oleic acid (1 g; 2 mmol, Aldrich, 90%) in benzyl ether (20 ml; Aldrich, 90%) to 300°C for 30 minutes. At 300°C, a severe reaction occurred and the solution became more turbid and brown-black; a sudden drop of about 15°C in the reaction temperature indicated the formation of nanocrystalline material. The resulting solution was cooled to room temperature after which 50 ml of ethanol was added to precipitate the nanocrystals. The nanocrystals were isolated by centrifugation and washed twice with ethanol and hexane.

Crystal structure of the nanocrystal product was confirmed via X-ray diffraction (XRD). Magnetization of the magnetite nanocrystals was measured at 298 K using a superconducting quantum interference device (SQUID; MPMS-XL, Quantum Design). Nanocrystal size was determined by transmission electron microscopy (Phillips, T12).

2.2 Fabrication of magnetic PLGA and cellulose particles

A known dry weight of magnetite nanocrystals was suspended in 2 ml of a 50 mg/ml solution of PLGA (I.V. ~0.67 dL/g, M_w ~40-75 kDa; Durect® Absorbables) or cellulose triacetate (44% acetyl, Sigma) in methylene chloride (Sigma). Magnetite feed ratios tested ranged from 13 to 50%, using PLGA and cellulose.

To fabricate PLGA microparticles, the magnetite-charged organic phase was then added dropwise to 4 ml of a 1% (w/v) aqueous solution of poly(vinyl alcohol) (PVA, 22 kDa, 88% hydrolyzed, Sigma) and homogenized at 24,000 rpm using an IKA® UltraTurrax homogenizer. The homogenized mixture was then added to 50 ml of distilled water and stirred for 3 hours in a chemical fume hood at room temperature with an overhead mechanical stirrer to allow for evaporation of methylene chloride. Particles were then isolated by centrifugation at 4,000 rpm for 10 minutes, washed thrice with distilled water, snap-frozen in liquid N_2, lyophilized and stored at -20°C.

To make PLGA nanoparticles, the initial organic phase was dispersed in 5% (w/v) PVA using a sonicator probe (work duty ~40%) and the resulting solution was added to 50 ml of 0.3% (w/v) PVA and allowed to stir for 3 hours as before. Cellulose nanoparticles were made by dispersing the initial organic phase in 1% (w/v) PVA using a sonicator probe (work duty ~40%) before adding to 50 ml of deionized water and stirring for 3 hours to enable solvent evaporation. Nanoparticles were isolated by centrifugation at 12,000 rpm for 6 minutes, washed thrice with distilled water, snap-frozen in liquid N_2, lyophilized and stored at -20°C.

Cellulose particles were regenerated by alkaline saponification of the cellulose triacetate particles [16]. This was done by suspending particles in methanol at a 1.4% (w/v) concentration, stirring at 40°C for 30 minutes, adding a 4% (v/v) equivalent of 5N NaOH and allowing the resulting mixture to stir for 5 hours. The regenerated particles were isolated by centrifugation at 10,000 rpm for 6 minutes, washed thrice with distilled water, snap-frozen in liquid N_2, lyophilized and stored at -20°C.

2.4 Characterization of magnetic PLGA and cellulose particles

2.4.1 Physicochemical and relaxometric analysis—Magnetic cellulose and poly(lactide-co-glycolide) particle morphology was analyzed via scanning electron microscopy (FEI XL-30, ESEM-FEG). The distribution of magnetite cores within the

polymeric matrix was analyzed by transmission electron microscopy (Phillips, T12). The particles were sized by using the formula: $D=2\times\sqrt{\frac{\text{Area}}{\pi}}$ to calculate particle diameters after using Image J software to analyze particle areas from representative SEM images. Loss of acetyl groups during regeneration of cellulose was observed using infrared spectroscopy (Nicolet 6700 FTIR).

Iron content of the magnetic polymer particles was determined using inductively coupled plasma–optical emission spectroscopy (Perkin-Elmer, Optima ICP-OES) after digestion in 36.5 wt% hydrochloric acid (Sigma).

To characterize surface charge and polydispersity, zeta potential measurements (ZetaPALS, Brookhaven Instruments) were collected manually on a 1% (w/v) suspension of magnetic polymer particles in water by averaging 10 runs, each composed of 12 cycles.

To measure r_2 and r_2* molar relaxivity, various concentrations of the magnetic polymer particles were resuspended in 1% (w/v) agarose (Sigma) and 0.2% (v/v) Gd-DTPA (Magnevist) to create gel phantoms at different iron concentrations. Transverse relaxation times were measured on a Bruker 4T magnet using multi-slice multi-gradient echo sequences and used to determine the relaxivities of the particles. The images at different echo times (TE) were reconstructed to fit the exponential signal decay curve: $S = S_0 e^{-(TE)R_2}$* in MATLAB and used to calculate the effective transverse relaxation rates (R_2, R_2*), where the R_2, R_2* and r_2, r_2* are related by: R_2, R_2* = [Fe]r_2, r_2* + $R_{2,0}$, $R_{2,0}$*.

2.4.2 Dissolution and degradation kinetics—The dissolution of polymer-entrapped magnetite was assessed using the standard infinite sink model used to assay drug release from drug delivery devices *in vitro*. Briefly, 1 mg of particles was suspended in 0.5 ml of either phosphate-buffered saline (1×PBS, pH 7.4; physiological mimic) or 50 mM sodium citrate buffer (pH 5.5; endolysosomal mimic) and placed in a rotary shaker at 37°C. Arbab et al, have previously used these buffers to analyze the decomposition of Ferumoxides [1]. At each time point, the sample was centrifuged, supernatant collected and replaced with fresh media. This was done in triplicate for each group of particles. Supernatant samples were analyzed for iron content using a Ferrozine-based colorimetric assay. Both samples and magnetite standards were treated with an equal volume of a 10% (w/v) saturated solution of hydroxylamine hydrochloride (Sigma) in concentrated HCl (36.5%, Sigma) prior to analysis.

The degradation of magnetic polymer particles was studied by measuring the evolution of r_2* over a period of about 30 days. To do this, 1 mg of particles was suspended in 0.5 ml of either 1×PBS (pH 7.4) or 50 mM sodium citrate buffer (pH 5.5) and placed in a rotary shaker at 37°C. At each time point, 10 μl of degrading particle suspension was taken out from sample tube, snap-frozen in liquid N_2 and stored at -20°C for later analysis. The remaining particle suspension was placed back in the rotary shaker at 37°C to continue degrading. This was also done in triplicate for each group of particles studied. Samples were thawed and resuspended in an aqueous solution of 1% (w/v) agarose and 0.2% (v/v) Gd-DTPA to make 250-μl phantoms. These were then imaged on a Bruker 4.7T magnet using a gradient echo sequence at multiple echo times. Since the [Fe] in the samples studied was kept constant, $R_2^* \propto r_2^*$; as such, the transient molar R_2* was used to track changes in r_2* relaxivity over time.

2.4.3 In vitro cytotoxicity—Cytotoxicity of magnetic polymer particles was assessed using the MTT assay. Human adenocarcinoma cells (MCF-7) and mouse mesenchymal stem cells (mMSCs) were treated with particles at three typical labeling concentrations corresponding to basis iron concentrations of 1 mM, 0.5 mM and 0.25 mM for 48 hours

using labeling media. Afterwards, the labeled cells were washed with 1×PBS and treated with 3-(4,5-dimethylthiazol-2-yl)-2,5-diphenyltetrazolium bromide, or MTT, for 3 h. The cells were then washed and treated with 1N HCl in isopropanol to solubilize MTT formazan present in cells. The formation of purple MTT formazan crystals, which absorb light at 540 nm, was measured on a spectrophotometer and used as a measure of cell viability. A negative control group was treated with 50 mM deoxyglucose and 15 mM sodium azide (a metabolic poison) for 48 hours (to deplete ATP levels within the cells) and used as a baseline.

2.5 Preparation and characterization of magnetically labeled cells

To characterize internalization of magnetic particles, mMSCs plated at uniform density were labeled at a basis [Fe] of 1 mM with magnetic polymer particles by mixing a warm 25 -μl stock of particles suspended in 1× PBS with 5 ml of DMEM media (10% fetal calf serum, 1% penicillin-streptomycin, 1% L-glutamine and 0.01 mg/ml insulin) and treating cells overnight with the labeling media. Fluorescent micrographs of labeled cells were acquired on a confocal fluorescence stereomicroscope (Leica). To do this, the magnetically labeled mMSCs were incubated in 1×PBS containing 1 μM of CM-DiI (Invitrogen) at 37°C for 10 mins to enable cytosolic staining, washed with 1× PBS to remove excess dye, resuspended in regular media and allowed to plate overnight at 37°C in chamber slides, fixed in 10% formalin and mounted in ProLong® Gold Anti-Fade reagent with DAPI (Invitrogen).

To determine the effectiveness of new particles to yield dark contrast by MRI, MCF-7 cells labeled according to the above procedure were suspended at 3 different cellular concentrations (5×10^5, 5×10^4 and 5×10^3 cells/ml) in 1% (w/v) agarose/0.2% (v/v) Gd-DTPA to create phantoms. T_2*-weighted gradient echo images of the labeled cell phantoms were then acquired at 3 echo times (2.4, 10 and 20 msecs) on a Bruker 4T magnet. Iron content of the labeled cells, as well as a sample of unlabeled cells, was determined using ICP-OES after digestion in 36.5 wt% hydrochloric acid (Sigma).

2.6 Data analysis and statistics

A one-way ANOVA with a Tukey post test was used to assess the statistical significance of differences observed in cell labeling efficiencies. A two-way ANOVA with a Bonferroni post test was used to assess the results of the MTT cytotoxicity study. A p value of $p < 0.05$ was considered to be statistically significant.

3. Results and Discussion

3.1 Physicochemical characterization of magnetite nanocrystals

10-nm magnetite nanocrystals with low size polydispersity were synthesized (Figure 1a). As shown in Figure 1b, the crystals displayed a characteristically high saturation magnetization (M_{sat}) of 72.1 emu/g with negligible remanence (2.69 emu/g or 3.4% of M_{sat}) upon being magnetized in a SQUID magnetometer, in close agreement with values previously observed [17] for magnetite crystals in their size range (10-15 nm). X-ray diffraction analysis showed close agreement between calculated and measured XRD patterns as shown in Figure 1c. Lattice fringe lines of the magnetic nanocrystals were visualized (inset, Figure 1a).

3.2 Characterization of magnetic PLGA and cellulose particles

Figure 2 shows scanning electron micrographs for magnetic PLGA nano- and microparticles. Also displayed is data for magnetic cellulose nanoparticles (Figure 2c). Magnetic PLGA particles were discrete, showing good spherical morphology and acceptable size distributions for both nano- (Figure 2a) and microparticles (Figure 2b). Magnetic cellulose particles were similarly discrete and spherical with acceptable polydispersity

(Figure 2c). Insets in each image are transmission electron micrographs of respective particles, showing uniform distribution of iron oxide cores in polymeric particles.

An analysis of magnetic content of the fabricated PLGA particles, as well as encapsulation efficiency is shown in Figure 3. Acid-terminated PLGA was found to encapsulate magnetite at much higher efficiencies than the ester-terminated variant for all feed ratios tested. Ester-terminated PLGA could only match the efficiency of the acid-terminated polymer at lower feed ratios. We believe this is caused by the strong electrostatic interaction known to occur between and Fe^{2+} and Fe^{3+} ions in magnetite and free carboxylic acid groups in substances like oleic acid. For this reason, oleic acid has long been proposed and used as an excipient for improving encapsulation efficiencies of magnetite in polymer composites with positive results [18]. The use of acid-terminated PLGA eliminates the need for an ancillary excipient, reducing the chemistry of a magnetic polymer composite to that of a simple, two-component system. Encapsulation efficiency, expressed as a percentage, was calculated using the following formula:

$$\frac{\text{Assayed } m_{Fe_3O_4} \text{ in sample (wt\%)}}{\text{Theoretical maximum } m_{Fe_3O_4} \text{ in sample (wt\%)}} \times 100\%$$

Encapsulation efficiency (as defined above) can be over 100% if all of the iron is incorporated within particles and there is some loss of polymer—as occurred during regeneration of the magnetic cellulose particles we made.

Figure 4 shows data on alkaline saponification (deprotection) of magnetic cellulose acetate particles and properties of both magnetic cellulose acetate and cellulose particles. As seen in Figure 4c, deprotection had little effect on particle morphology. FTIR spectra of cellulose acetate particles shows a sharp ester carbonyl (C = O) peak at $1745cm^{-1}$. After deprotection, this peak is absent, concurrent with the appearance of a broad hydrogen-bonded hydroxyl (O – H) peak at $3366cm^{-1}$. This confirms the loss of acetyl groups and regeneration of free hydroxyls as present in native cellulose. Besides causing a 22.5% reduction in particle diameter and a consequent 25% increase in the weight fraction of iron present in the resulting cellulose particles, the deprotection did little else to disturb the integrity of the magnetic cellulose composites.

The measured molar relaxivities of the various polymeric contrast agents made are listed in Table 1 alongside those of Feridex®, an FDA-approved contrast agent commonly used for magnetic cell labeling. For all particles studied, both r_2 and r_2* per millimole of particles for micron-sized particles were substantially higher than those of nano-sized agents. The r_2* values were 2 to 14 times as high as their respective r_2 values, with the disparity being largest in the micron-sized particles. This observation is consistent with the current body of theoretical work describing the relaxivity behavior of a superparamagnetic contrast agent as a function of its size in the static dephasing regime [20], where the contribution of static magnetic field offset to nuclear spin dephasing in the transverse plane by far supersedes any effects of diffusion through magnetic field gradients. The high iron content of the polymeric agents coupled with the presence of a thin polymer coating allows close proximity of protons to the superparamagnetic iron oxide cores, enhancing the r_2* of the overall composite.

3.3 Dissolution kinetics of magnetic PLGA and cellulose particles

The dissolution of iron over time was assayed by incubating magnetic particles in citrate buffer over 100 days and measuring the solubilized iron. Citrate buffer was used to mimic

the lysosomal environment to which particles are exposed following endocytosis by cells. Magnetic PLGA particles display characteristic dissolution profiles for the release of a solute from an erodible matrix [21]. There is an initial 'burst' phase, during which most of the iron on the surface of the particles gets dissolved. This is followed by a gentle plateau during which most of the PLGA in both the micro- and nanoparticles degrades by bulk hydrolysis. The duration of this phase is dependent on the size of the particle and the molecular weight of PLGA. Since both micro- and nanoparticles were made with the same molecular weight PLGA, the faster dissolution observed in nanoparticles owes mainly to their smaller size, and higher surface area-to-volume ratio. The higher surface area-to-volume ratio also severely limits the encapsulation efficiency of nanoparticles as observed in Figure 3. As shown in Figure 5a, after 30 days, while a little over 30% of the iron in the magnetic PLGA nanoparticles is solubilized in citrate buffer, only 10% of the iron content of the microparticles is dissolved. The lower surface area-to-volume ratio of the microparticles allows for slower degradation, which means that the micron-sized magnetic PLGA composites remain intact much longer. The micro- and nanoparticles are both completely degraded after 100 days, even though the nanoparticles degrade at a much faster rate. After 1 day, the microparticles lose 3% of their iron content due to dissolution, while the nanoparticles lose as much as 21% in the same time frame. After all of the PLGA degrades, the free magnetite cores are exposed directly to the buffer and dissolve at a rate that is independent of the PLGA. This is illustrated clearly by the data in Figure 5a as a third phase characterized by a steep ascent in the amount of dissolved iron.

Magnetic cellulose particles have a strikingly different dissolution profile from that of their PLGA counterparts as seen in Figure 5b. After 30 days in citrate buffer, the cellulose particles lose about 35% of their iron content in citrate buffer through a first-order dissolution profile. The cellulose acetate particles, on the other hand, show similar dissolution kinetics to the PLGA nanoparticles, with the exception of a slower 'burst' phase with only about 12% of the iron content lost after 1 day. The difference between the dissolution profiles of cellulose and cellulose acetate is caused by the more negative zeta potential of the cellulose acetate particles. The deprotection procedure used to regenerate the cellulose particles also removes much of the surface iron oxide as the particles become 23% smaller in diameter and experience a 53% loss in volume due mostly to the removal of the acetate groups. Furthermore, the dissolution kinetics of cellulose and cellulose acetate are swelling-controlled [21]. Cellulose particles swell to a greater extent in water than cellulose acetate particles over a relatively short period of time. This swelling behavior significantly affects the transport mechanics of iron from inside cellulose particles, dramatically slowing the rate of dissolution. A model of swelling-controlled release has been described by Lee and Peppas [22].

Citrate buffer was used to mimic the acidic milieu of a lysosome, the principal site of magnetic labeling in our study. Most drug delivery studies use PBS to mimic the extracellular, physiological environment of cells. Since it is generally known that cells treated with particulate agents tend to endocytose them, perhaps studying drug release in both citrate buffer and PBS would provide more wholesome information on how a drug delivery agent behaves *in vitro*. To emphasize this point, a similar dissolution study was performed using PBS. The dissolution of iron in PBS was negligible for all sets of particles investigated. Under 12% of the iron content in all the particles studied was solubilized after 85 days.

3.4 Degradation kinetics of magnetic PLGA and cellulose particles

Physical degradation of the magnetic polymer particles was assayed by incubating magnetic particles in citrate buffer and PBS for 100 days and measuring r_2* molar relaxivity. Magnetic PLGA particles display a rapid decline in r_2* molar relaxivity within the first two

weeks, followed by a gradual reduction after 50 days. This was the case for both nano- and microparticles. Magnetic cellulose particles, on the other hand, had much less initial reduction in r_2* and exhibited less of a decline in r_2* values overall, retaining as much as 85% of their initial relaxation rates after 50 days. These trends are portrayed in Figure 6.

For all agents studied, the decline in relaxivity was more rapid in citrate buffer than in PBS due to the dissolution of iron oxide cores. The relative enhancement in residual r_2* observed in PLGA nanoparticles occurs because of the rapid rate at which the PLGA nanoparticles degrade. The free cores that remain after degradation tend to aggregate, and this is reflected as a temporary enhancement in r_2*. The PLGA microparticles degrade more slowly and have a more delayed and attenuated aggregation peak.

While the PLGA samples became clear within weeks of degrading, the cellulose samples remained turbid for the entire duration of the study. Cellulose is known to degrade only under harsh acidic conditions or in the presence of enzymes. As such any change in the relaxation rate can only be attributed to the swelling of cellulose particles. Since swelling increases the size of the particles while widening the distance between magnetite cores, one would expect it to reduce the r_2* relaxivity, diluting the strength of a cellulosic contrast agent. The negative effect of swelling on relaxivity would only be enhanced by the dissolution of the cores, which occurs simultaneously. On the other hand, the rush of water molecules into the cellulosic matrix during swelling enables protons to have better access to the iron oxide cores that make up a composite particle, thereby enhancing the magnetic susceptibility effect of the cellulosic agents and, by extension, its r_2*.

These antagonistic processes help explain the differences observed between the degradation profiles of cellulose and cellulose acetate particles. Since the cellulose acetate agent shows a faster dissolution of iron content, its residual molar r_2* is mostly lower than that of cellulose in the early time points, showing a definite decline after a week to about 50% of its original value. Because the cellulose agent has a much slower, first-order dissolution profile for its iron content, both processes come into play. The drop in residual r_2* seen after a week can be attributed to the negative effect of swelling and the subsequent plateau observed in the following 2 weeks can be attributed to the increased water content of the cellulose particles after swelling. The steady decline of r_2* values observed in citrate buffer from then on is due to the dissolution of iron oxide cores.

3.5 Cytotoxicity of PLGA and cellulose particles

Using the MTT assay, magnetic PLGA and cellulose particles were shown to have no toxic effects on either mMSCs or MCF-7 cells at all three basis iron concentrations used in cell labeling (1 mM, 0.5 mM and 0.25 mM). Cells labeled for 48 hours with magnetic PLGA and cellulose particles had a survival rate of 96 to 182% relative to untreated control cells, as shown in Figure 7. Cells treated with magnetic particles seemed to have a higher survival rate than those treated with blank control particles because of the higher metabolic activity of the magnetically labeled cells. Since the MTT assay uses mitochondrial activity as a measure of cell viability, cells loaded with iron would tend to expend more energy as they actively metabolize iron. In contrast, those loaded with blank polymer had a slightly lower “survival” rate relative to the untreated control. More detailed viability and cell differentiation assays are underway; however, the general non-toxicity of these types of particles seems clear.

3.6 Magnetic labeling of cells with PLGA and cellulose particles

Figure 8 shows (confocal) fluorescent micrographs of mesenchymal stem cells labeled with fluorescent versions of PLGA and cellulose nano- and microparticles, as well as with non-

fluorescent Feridex®. These images show considerable labeling of cells with all of the different polymeric contrast agents studied. For cells labeled with PLGA and cellulose agents, confocal microscopy was used to confirm internalization of the particles. Quantification of iron content within the cells by ICP analysis revealed significantly high iron content in cells labeled overnight with all particle types studied (Figure 9a). The high cellular iron of the Feridex® group was only achieved with the use of the transfection agent, poly-L-lysine. While Feridex® had to be complexed with poly-L-lysine in order to be used effectively, none of the PLGA or cellulose particles required the use of a transfection agent.

Even without the use of a transfection agent, PLGA microparticles show a much higher labeling efficiency per millimole of iron than Feridex®/PLL as indicated by a higher iron content per labeled cell. Cells labeled with PLGA microparticles contained almost as much iron as those labeled with Bangs®. Similarly, cellulose nanoparticles had a higher labeling efficiency than PLGA nanoparticles. A multitude of factors could explain these results. Key among these is that the bigger and heavier particles sink easily in the labeling media and have rapid contact with plated cells.

A more positive zeta potential should also enhance the labeling efficiency since the membrane potential of a cell is negative; this explains why poly-L-lysine, which has a very positive zeta potential, is used as a transfection agent. The relatively higher labeling efficiency of cellulose nanoparticles ($\zeta = -11.4 \pm 0.8$ mV) when compared with those of cellulose acetate ($\zeta = +8.9 \pm 0.6$ mV) or PLGA ($\zeta = -9.7 \pm 1.1$ mV) nanoparticles, however, seems to contradict this claim. Our results, therefore, suggest that the hydrodynamic size of the contrast agent (either as a single, opsonized particle or as an aggregated mass of them) as it interacts with the cell is the more limiting factor when explaining differences in cell labeling efficiency.

Lastly, MRI was performed on cell samples labeled with either magnetic PLGA nanoparticles, Feridex® or blank PLGA particles. Figure 9b is a set of T_2*-weighted gradient echo images acquired at 3 echo times (2.4, 10 and 20 msecs), showing loss in signal observed at three different concentrations (5×10^5, 5×10^4 and 5×10^3 cells/ml) of MCF-7 cells labeled with magnetic PLGA particles, Feridex® and blank PLGA particles. At the same cellular concentrations, neither Feridex labeled cells, nor blank PLGA particle labeled cells displayed significant hypointense contrast. The dramatic loss of signal observed in the T_2*-weighted image of cells labeled with magnetic PLGA illustrates the utility of using these particles as contrast agents for MR-based cell tracking.

As evident from the dissolution and degradation studies, two separate classes of biodegradable contrast agents have been fabricated: one that degrades fast (PLGA) and one with slower degradation kinetics (cellulose). Short-lived agents could be used to track immune cells, which have a lifespan on the order of days. Longer-lived agents, on the other hand, could be used to track stem cells, which have a much longer life cycle. Nanoparticles and microparticles would further have specific, independent uses. For example, cells that grow in suspension, such as T-lymphocytes or hematopoietic stem cells, typically have little cytoplasm, which may preclude robust labeling with microparticles.

4. Conclusion

Biodegradable, fluorescent and magnetic particles of cellulose and PLGA were fabricated. Particles encapsulated high levels of magnetite and exhibited very high r_2* molar relaxivities. Both PLGA and cellulose based nano- and microparticles robustly labeled cells and were non-toxic. PLGA and cellulose based particles degraded at very different rates, enabling selective use of either slow- or fast-degrading particles for particular biological

studies. As both polymers are FDA-approved, and *in vitro* assays confirmed iron dissolution in endosomal mimicking solutions, these new classes of particles have a clear trajectory for clinical translation.

Acknowledgments

The authors would like to thank Dr. Christoph Rahner for his assistance with TEM, Dr. Yosi Bason for assistance with SQUID magnetometry and Dr. Dorit Granot for helpful discussions on MR theory. Dr. Shouheng Sun is greatly thanked for teaching us how to synthesize metal oxide cores. Financial support from NIH grants P30 NS052519 and DP2 OD004362 is acknowledged.

References

1. Arbab AS, Wilson LB, Ashari P, Jordan EK, Lewis BK, Frank JA. A model of lysosomal metabolism of dextran coated superparamagnetic iron oxide (SPIO) nanoparticles: implications for cellular magnetic resonance imaging. NMR in Biomedicine. 2005 Oct; 18(6):383–389. [PubMed: 16013087]
2. Arbab AS, Yocum GT, Wilson LB, Parwana A, Jordan EK, Kalish H, Frank JA. Comparison of transfection agents in forming complexes with ferumoxides, cell labeling efficiency, and cellular viability. Molecular Imaging. 2004 January; 3(1):24–32. [PubMed: 15142409]
3. Hsiao J, Tai M, Chu H, Chen S, Li H, Lai D, Hsieh S, Wang J, Liu H. Magnetic nanoparticle labeling of mesenchymal stem cells without transfection agent: Cellular behavior and capability of detection with clinical 1.5 T magnetic resonance at the single cell level. Magnetic Resonance in Medicine. 2007 Oct; 58(4):717–724. [PubMed: 17899592]
4. Shapiro EM, Skrtic S, Koretsky AP. Sizing it up: Cellular MRI using micron-sized iron oxide particles. Magnetic Resonance in Medicine. 2005 Feb; 53(2):329–338. [PubMed: 15678543]
5. Walczak P, Kedziorek D, Gilad A, Barnett B, Bulte J. Applicability and limitations of MR tracking of neural stem cells with asymmetric cell division and rapid turnover: The case of the Shiverer dysmyelinated mouse brain. Magnetic Resonance in Medicine. 2007 Aug; 58(2):261–269. [PubMed: 17654572]
6. Shapiro EM, Sharer K, Skrtic S, Koretsky AP. In vivo detection of single cells by MRI. Magnetic Resonance in Medicine. 2006 Feb; 55(2):242–249. [PubMed: 16416426]
7. Hinds KA, Hill JM, Shapiro EM, Laukkanen MO, Silva AC, Combs CA, Varney TR, Balaban RS, Koretsky AP, Dunbar CE. Highly efficient endosomal labeling of progenitor and stem cells with large magnetic particles allows magnetic resonance imaging of single cells. Blood. 2003 August 1; 102(3):867–872. [PubMed: 12676779]
8. Bowen CV, Zhang X, Saab G, Gareau PJ, Rutt BK. Application of the static dephasing regime theory to superparamagnetic iron-oxide loaded cells. Magnetic Resonance in Medicine. 2002 July; 48(1):52–61. [PubMed: 12111931]
9. Shapiro EM, Skrtic S, Sharer K, Hill JM, Dunbar CE, Koretsky AP. MRI detection of single particles for cellular imaging. Proceedings of the National Academy of Sciences of the United States of America. 2004 July 27; 101(30):10901–10906. [PubMed: 15256592]
10. Bulte, J. Nanoparticles in biomedical imaging : emerging technologies and applications. New York NY: Springer; 2008.
11. Lee ES, Shuter B, Chan J, Chong MS, Ding J, Teoh S, Beuf O, Briguet A, Tam KC, Choolani M. The use of microgel iron oxide nanoparticles in studies of magnetic resonance relaxation and endothelial progenitor cell labelling. Biomaterials. 2010 Apr; 31(12):3296–3306. [PubMed: 20116846]
12. Wang L, Neoh K, Kang E, Shuter B, Wang S. Biodegradable magnetic-fluorescent magnetite/poly(dl-lactic acid-co-α,β-malic acid) composite nanoparticles for stem cell labeling. Biomaterials. 2010 May; 31(13):3502–3511. [PubMed: 20144844]
13. Lim YT, Noh Y, Han JH, Cai Q, Yoon K, Chung BH. Biocompatible Polymer-Nanoparticle-Based Bimodal Imaging Contrast Agents for the Labeling and Tracking of Dendritic Cells. Small. 2008 Oct; 4(10):1640–1645. [PubMed: 18819168]

14. Park J, An K, Hwang Y, Park J, Noh H, Kim J, Park J, Hwang N, Hyeon T. Ultra-large-scale syntheses of monodisperse nanocrystals. Nature Materials. 2004 Nov; 3(12):891–895.
15. Park J, Joo J, Kwon S, Jang Y, Hyeon T. Synthesis of Monodisperse Spherical Nanocrystals. Angewandte Chemie International Edition. 2007 Jun; 46(25):4630–4660.
16. Ikada Y, Tabata Y. Phagocytosis of Bioactive Microspheres. Journal of Bioactive and Compatible Polymers. 1986 Jan; 1(1):32–46.
17. Lee J, Huh Y, Jun Y, Seo J, Jang J, Song H, Kim S, Cho E, Yoon H, Cheon J. Artificially engineered magnetic nanoparticles for ultra-sensitive molecular imaging. Nature Medicine. 2007 January; 13(1):95–99.
18. Senpan A, Caruthers SD, Rhee I, Mauro NA, Pan D, Hu G, Scott MJ, Fuhrhop RW, Gaffney PJ, Lanza GM. Conquering the Dark Side: Colloidal Iron Oxide Nanoparticles. ACS Nano. 2009 Dec; 3(12):3917–3926. [PubMed: 19908850]
19. Luo X, Liu S, Zhou J, Zhang L. In situ synthesis of Fe3O4/cellulose microspheres with magnetic-induced protein delivery. Journal of Materials Chemistry. 2009; 19(21):3538.
20. Muller RN, Gillis P, Moiny F, Roch A. Transverse relaxivity of particulate MRI contrast media: From theories to experiments. Magnetic Resonance in Medicine. 1991 Dec; 22(2):178–182. [PubMed: 1812343]
21. Arifin DY, Lee LY, Wang C. Mathematical modeling and simulation of drug release from microspheres: Implications to drug delivery systems. Advanced Drug Delivery Reviews. 2006 November 30; 58(12-13):1274–1325. [PubMed: 17097189]
22. Lee PI, Peppas NA. Prediction of polymer dissolution in swellable controlled-release systems. Journal of Controlled Release. 1987 Dec; 6(1):207–215.

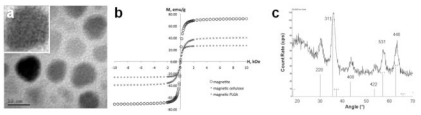

Figure 1.

Properties of synthesized magnetic nanocrystals. (a) HRTEM image showing 10-nm cores; inset, image of a single nanocrystal showing crystal lattice fringes; scale bar: 10 nm. (b) Hysteresis loop of synthesized magnetite cores (alongside those of magnetic polymer composites) showing high M_{sat} and negligible remanence. (c) X-ray diffraction of magnetite cores. Measured spectrum for synthesized cores appears above calculated diffraction peaks for magnetite.

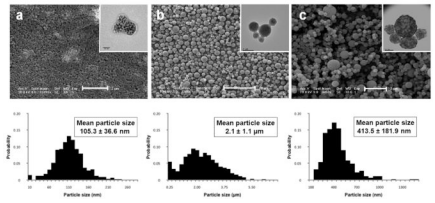

Figure 2.

Microscopic images and size distributions of magnetic polymer particles: SEM micrographs with inset TEM images showing inner distribution of iron oxide cores and histograms (below) showing particle size distributions. (a) magnetic PLGA nanoparticles, (b) magnetic PLGA microparticles, and (c) magnetic cellulose nanoparticles.

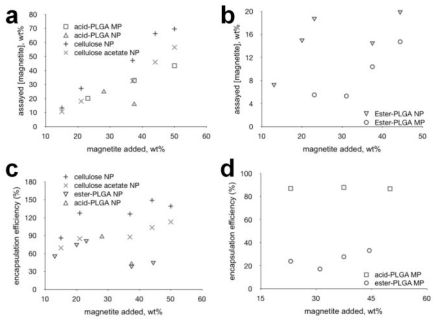

Figure 3.

Magnetite encapsulation efficiencies for PLGA and cellulose. (a) acid-terminated PLGA micro-/nanoparticles and cellulosic nanoparticles (b) ester-terminated PLGA micro- and nanoparticles. (c) encapsulation efficiencies of nanoparticles made using cellulose, acid- and ester-terminated PLGA. (d) encapsulation efficiencies of microparticles made using acid- versus ester-terminated PLGA. assayed [magnetite] = mass fraction of magnetite in wt%

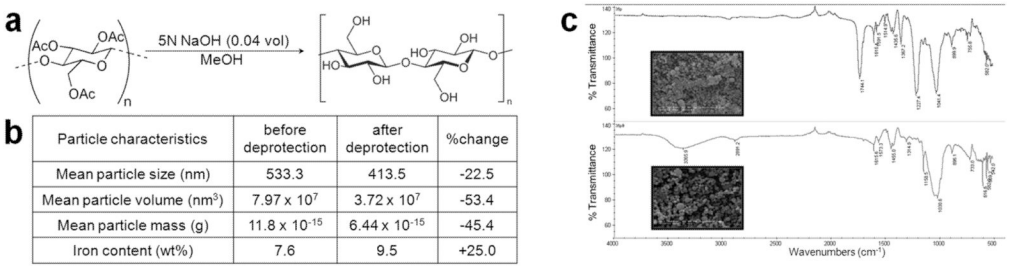

b

Particle characteristics	before deprotection	after deprotection	%change
Mean particle size (nm)	533.3	413.5	-22.5
Mean particle volume (nm^3)	7.97×10^7	3.72×10^7	-53.4
Mean particle mass (g)	11.8×10^{-15}	6.44×10^{-15}	-45.4
Iron content (wt%)	7.6	9.5	+25.0

Figure 4.

Regeneration of magnetic cellulose nanoparticles. (a) schematic of alkaline saponification reaction (b) table detailing physical changes observed post-deprotection (c) FTIR spectra of magnetic cellulose acetate particles (top) and regenerated magnetic cellulose particles (bottom) with inset SEM pictures.

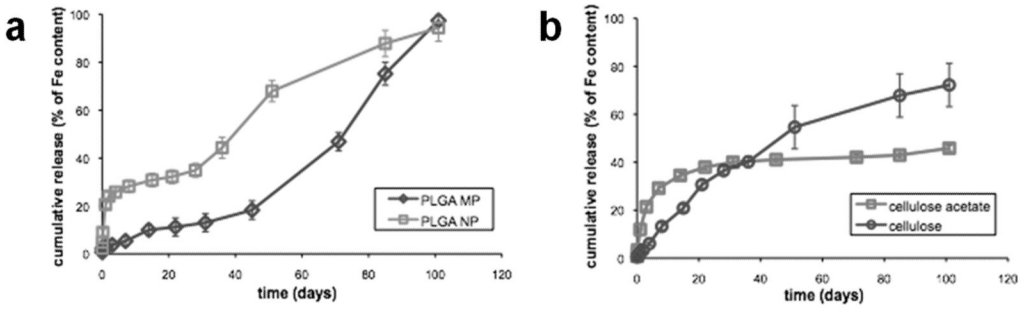

Figure 5.

Dissolution profile of magnetic polymer particles in citrate buffer. 100-day dissolution study of (a) magnetic PLGA and (b) magnetic cellulose nanoparticles, in citrate buffer (pH 5.5).

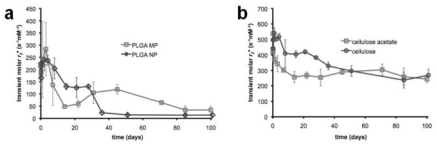

Figure 6.
Degradation study of magnetic polymer particles in citrate buffer. 100-day degradation study of (a) magnetic PLGA and (b) magnetic cellulose nanoparticles, in citrate buffer (pH 5.5).

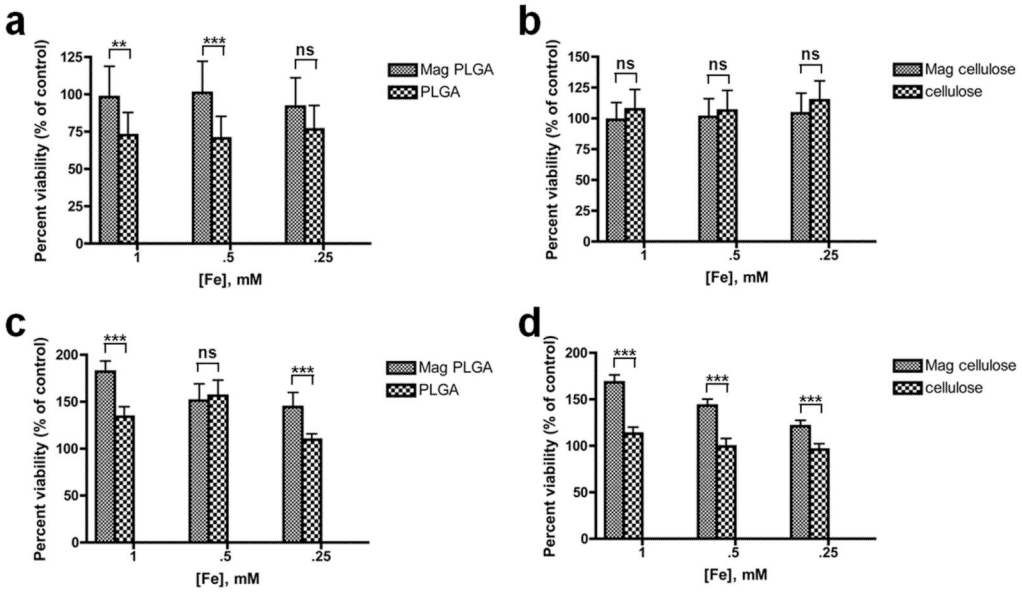

Figure 7.

MTT cytotoxicity assay performed on MCF-7 cells using (a) magnetic PLGA particles and (b) magnetic cellulose particles; and on mMSCs using (c) magnetic PLGA particles and (d) magnetic cellulose particles.

*** extremely significant ($p < 0.001$), ** very significant ($0.001 < p < 0.01$), *significant ($0.01 < p < 0.05$), ns = no significant difference ($p > 0.05$).

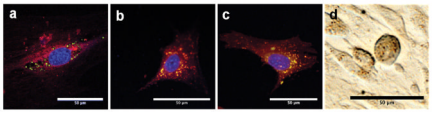

Figure 8.

High-magnification images of mesenchymal stem cells labeled with (a) PLGA microparticles, (b) PLGA nanoparticles, (c) cellulose nanoparticles, and (d) Feridex®. scale bar: 50μm. (a), (b) and (c) were taken on confocal fluorescent microscope. Cell bodies are stained red with CM-DiI, a lipophilic dye. Internalized coumarin-6-doped magnetic particles fluoresce green, and in the case of (b) and (c), are seen as yellow spots due to the colocalization of CM-DiI (red) and internalized particles (green) in endosomes. This effect is not seen in (a) due to the relatively high amounts of coumarin-6 dye in the microparticles; (d) was taken with unfiltered white light on an inverted microscope.

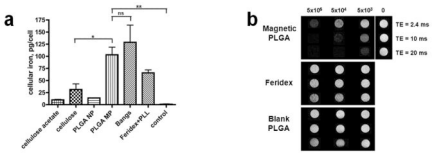

Figure 9.

Cell labeling efficiency of magnetic polymer particles (a) iron content of mesenchymal stem cells labeled with various contrast agents investigated (b) T_2*-weighted MRI of MCF-7 cells labeled with magnetic PLGA particles.

** very significant ($0.001 < p < 0.01$), *significant ($0.01 < p < 0.05$), ns = no significant difference ($p > 0.05$).

Table 1

Relaxometry of polymeric contrast agents

Particle characteristics	cellulose	cellulose acetate	ester-terminated PLGA		acid-terminated PLGA		Feridex®	Bangs beads
Particle size range	nano	nano	nano	micro	nano	micro	nano	micro
Particle size, nm	413.5	533.3	130	1500	105	2100	150	1600
Zeta potential (pH 7.0), mV	-11.4 ± 0.8	+8.9 ± 0.6	-12.7 ± 0.5	-21.3 ± 0.6	-9.7 ± 1.1	-18.8 ± 0.7	-6.7 ± 0.6	-32.3 ± 0.6
Magnetite content, wt%	69.6	56.4	15.3	5.1	24.7	43.3	0.19	42.5
r_2 per mmol Fe, $s^{-1}mM^{-1}$	62.81	75.1	83.8	93.1	269.8	20.9	110.5	52.7
r_2* per mmol Fe, $s^{-1}mM^{-1}$	398.6	399.0	262.6	554.5	505.0	261.0	214.8	454.7
r_2 per mmol particles[a] ($\times 10^{10}$), $s^{-1}mM^{-1}$	3.73	5.82	0.0172	9.08	0.0513	66.6	0.000298	58.9
times *better* than[b] Feridex®	12500	19500	57.6	30500	172	224000	1	198000
r_2* per mmol particles ($\times 10^{10}$), $s^{-1}mM^{-1}$	23.7	30.9	0.0538	54.1	0.096	832	0.000579	508
times *better* than Feridex®	40900	53400	92.9	93400	166	1440000	1	878000

[a] 1 mmol of particles = 6.02×10^{20} particles

[b] ratios are rounded to 3 significant figures